



Temperature- and degree of cure-dependent viscoelastic properties of photopolymer resins used in digital light processing

T. Rehbein¹ · M. Johlitz¹ · A. Lion¹ · K. Sekmen² · A. Constantinescu²

Received: 5 February 2021 / Accepted: 2 June 2021 / Published online: 21 June 2021
© The Author(s) 2021

Abstract

In the present paper, the degree of cure-dependent viscoelastic properties of a commercial photopolymer resin (Loctite® 3D 3830) used in digital light processing (DLP) 3D printing are investigated experimentally and described by suitable model equations. To do this, tests are carried out both on the liquid resin and printed specimens under various conditions. The experimental methods include photo-DSC, UV rheometry, and dynamic mechanical analysis. A commercial digital light processing (DLP) printer (Loctite® EQ PR10.1) is used for the printing of the samples. Model equations are proposed to describe the behavior of the material during and after the printing process. For the representation of the degree of cure depending on temperature and light intensity, the one-dimensional differential equation proposed in a previous paper is extended to capture a temperature-dependent threshold value. The change of the viscoelastic properties during crosslinking is captured macroscopically by time-temperature and time-cure superposition principles. The parameters of the model equations are identified using nonlinear optimization algorithms. A good representation of the experimental data is achieved by the proposed model equations. The findings of this paper help users in additive manufacturing of photopolymers to predict the material properties depending on the degree of cure and temperature of printed components.

Keywords Photopolymer · Viscoelastic modeling · Temperature-dependent behavior · UV-curing · Digital light processing

1 Introduction

During the last 3 decades, additive manufacturing (AM) processes for polymers have undergone rapid development from prototyping to small- and medium-sized production. Currently, a broad range of methods exists for the product generation layer by layer, which contains liquid, solid or powdery materials as a basis. Depending on the chemical structure, i.e., thermoplastic or thermoset, the raw material is either crosslinked or melted by the AM process. In the case of thermoplastics, the material is melted by a heated extruder head (fused filament fabrication) or by a laser beam (selective laser sintering), whereas with thermosetting

resins, a crosslinking reaction is started by incident UV or thermal radiation. However, this paper does not consider thermoplastics but discusses the change of viscoelastic properties of thermosetting photopolymer resins cured by UV irradiation in additive manufacturing.

Generally, photopolymer resins are used in additive manufacturing processes like digital light processing (DLP) and stereolithography (SLA). The liquid resin is cured by UV irradiation (typically emitted by a UV LED working at a wavelength of $\lambda = 405$ nm) and built up layerwise to the desired geometry. This process is accompanied by a phase change: the photoinitiator reacts due to UV irradiation and starts the crosslinking process of the monomers and oligomers.

Figure 1 shows the general setup of a DLP 3D printer. The liquid photopolymer is filled into the resin tray manually or automatically before starting the printing process. A transparent glass window is attached to the bottom of the resin tray that is permeable to the UV irradiation emitted by the projector. The projector flashes an image on the resin tray that has been previously created in a slicing process using a CAD file. After irradiation, the photopolymer resin

✉ T. Rehbein
rehbein@unibw.de

¹ Department of Aerospace Engineering, Institute of Mechanics, Bundeswehr University Munich, Werner-Heisenberg-Weg 39, 85577 Neubiberg, Germany

² Laboratoire de Mécanique des Solides, CNRS, École Polytechnique, Institut Polytechnique de Paris, Route de Saclay, 91120 Palaiseau, France

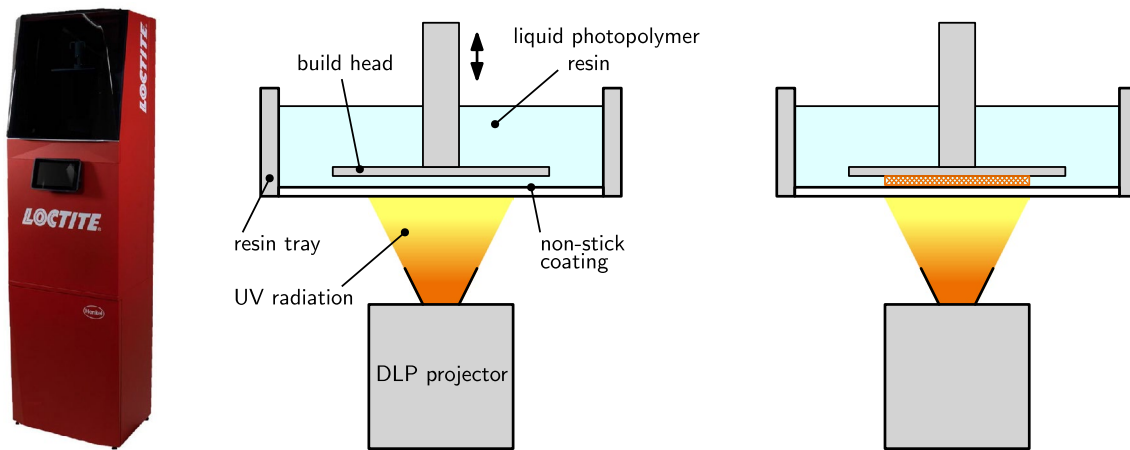


Fig. 1 Left: Loctite® EQ PR10.1 DLP 3D printer. Center: schematic representation of digital light processing and description of the components. Right: crosslinking of the first layer

layer is cured and adheres to the build plate as well as to the glass window of the resin tray that is coated with a non-stick coating to peel the cured layer from the resin tray. The radiation step is repeated until the completion of the print job. After finishing the print job, the printed part is washed in isopropanol to remove the excessive resin and post-cured in a curing chamber with UV irradiation to achieve the final properties.

Due to the general increase of research activities in the field of additive manufacturing, the experimental characterization and description of the material behavior of photopolymer resins with suitable model equations have been of high relevance. These investigations include all steps of the entire AM process chain:

- Design and development of customized photopolymer resins for specific applications [1]
- Identification and quantification of relevant process parameters (e.g., layer thickness, exposure time, and light intensity) [2]
- Phenomenological modeling of the macroscopic behavior of printed parts during and after the printing process using continuum mechanics [3–7]
- Influence of post-curing treatments on the mechanical properties [8–10]
- Simulation and prediction of the printing process and following load cases [11, 12].

For the numerical simulation of the additive manufacturing of photopolymer resins, experimentally validated material models are necessary to predict the material behavior during and after the printing process.

Several phenomena occur during the printing process and, during the transition from a fluid to a solid, an increase in the degree of cure occurs:

- Change of viscoelastic properties depending on frequency, temperature, and degree of cure [13]
- Chemical shrinkage leading to warpage of printed parts and distortion of the desired properties [14, 15]
- Decrease of elongation at break as well as increase in tensile strength and stiffness [16, 17].

In detail, this paper will focus on the first phenomenon mentioned and will show experimental techniques as well as modeling approaches to cover and predict these dependencies. The consideration of the material behavior during the printing process is important for a successful print job. To mention a few, lacking knowledge about curing shrinkage, stiffness increase due to progressing crosslinks, and heat generation in the resin can lead to geometric deviations, fracture of layers, and gradients in the degree of cure of the printed geometry. In particular, it will be shown that the viscoelastic properties of the photopolymer show a strong presence during and after the curing process and that the assumption of linear-elastic material behavior is insufficient.

The Loctite® EQ PR10.1 DLP 3D printer (build size: 192 x 108 x 250 mm) is used for the fabrication of the samples used in this paper (see Fig. 1). It consists of a full HD (1920 x 1080 pixels) projector, which emits UV radiation at a wavelength of 405 nm by an LED. This open system enables the usage of all third-party photopolymer resins that cure at a wavelength of 405 nm as well as the adjustment of all relevant process parameters (layer thickness, exposure time, irradiance, etc.).

In addition to the aforementioned process parameters, the temperature of the resin during the printing process has a significant influence on the crosslinking behavior and the resulting mechanical properties. Recent publications have shown that the temperature-controlled printing of photopolymers at elevated temperatures leads to the same mechanical

properties of the printed specimens compared to those that were printed at room temperature and post-cured afterwards using a UV chamber [18, 19]. Furthermore, the authors have discovered that a resin tray with integrated temperature control enables a better processing of highly viscous photopolymer resins.

2 Experimental characterization and modeling of the crosslinking reaction

The investigated material is the Loctite® 3D 3830 photopolymer resin, which is acrylate-based and used for the production of prototypes. Based on the safety data sheet [20], it consists of 80–90 % (Octahydro-4,7-methano-1H-indenedyl) bis(methylene) diacrylate and has a transparent appearance.

Photo-DSC measurements are conducted to investigate the crosslinking reaction of photopolymers. In a recent publication [21], the crosslinking reaction of the Loctite® 3D 3830 photopolymer resin was investigated experimentally using Photo-DSC under several isothermal conditions. To do this, a conventional TA Instruments® Q2000 DSC has been upgraded with the OmniCure® S2000 UV-curing system.

The variables that most influence the curing process are light intensity \mathcal{I} and temperature θ . To gain a deeper insight into the working principle of photo-DSC measurements, the reader is referred to [21].

The DSC measures the heat flow that is released by the photopolymer sample during the exothermal crosslinking reaction. The degree of cure $q(t)$ is then calculated as the ratio between accumulated released heat and the total heat of reaction of the fully crosslinked material

$$q(t) = \frac{\int_0^t \dot{h}(\bar{t}) d\bar{t}}{h_{\text{tot}}}. \quad (1)$$

The degree of cure is dimensionless and ranges from 0 (liquid) to 1 (fully cured). Several samples have been investigated under the influence of two light intensities (5 and 10 mW/cm²) and seven constant temperatures (−10...50 °C in 10 °C steps). The broad temperature range is necessarily chosen, because the filled-in resin can substantially heat up due to the exothermic reaction of the adjacent resin that crosslinks in the exposed area of the resin tray. The total heat of the reaction h_{tot} has been determined by heating a photopolymer sample from 20 °C to 70 °C at 5 °C/min and simultaneously irradiating with 10 mW/cm². In the second photo-DSC scan with the same experimental conditions using the same specimen, no more exothermic reaction was visible.

The experimental results of the photo-DSC measurements for the aforementioned test conditions are depicted as dots in Fig. 2. Based on the experimental results, a strong influence

of the isothermal test condition was observed. Additionally, the photopolymer reaches a temperature-dependent threshold value for the degree of cure at the end of the irradiation, which has to be taken into account in the following section.

The phenomenological differential equation for the evolution of the degree of cure has been published in [21] and is based on the model developed by Kamal and Sourour [22], which has proven best practice for the modeling of curing processes of polymers in general [23–25]

$$\dot{q} = (k_1 + k_2 q^m)(q_{\text{max}} - q)^n. \quad (2)$$

Compared to [21], the equation is extended by the temperature-dependent threshold value q_{max}

$$q_{\text{max}}(\theta) = \frac{1}{1 + \exp(-a_0(T - T_0))}. \quad (3)$$

The Arrhenius type coefficients k_1 and k_2 depend on the absolute temperature T as well as on light intensity \mathcal{I} and read as follows:

$$k_i = A_i \exp\left(-\frac{E_i}{RT}\right) \left(\frac{\mathcal{I}}{\mathcal{I}_{\text{ref}}}\right)^b. \quad (4)$$

The constant reference value $\mathcal{I} = 1 \text{ mW/cm}^2$ is merely used to ensure unit consistency with the pre-exponential factors A_i and to avoid unmanageable units. Moreover, R and E_i denote the universal gas constant and activation energies, respectively.

The parameters of the model equation for the degree of cure q are identified simultaneously with regard to all 14 photo-DSC measurements using the commercial optimization program LS-OPT®. The comparison between the model prediction and the experimental results is displayed in Fig. 2, and the corresponding model parameters are listed in Table 1. It should be noted that the listed parameters differ from the parameters determined in the previous work [21] as Eq. 3 has additionally been inserted into the model equation.

In summary, it can be seen that the model captures the experimental behavior very well leading to a summarized mean squared error of 0.028. Only the experimental data under the conditions $\mathcal{I} = 10 \text{ mW/cm}^2$, $\theta = 20 \text{ °C}$ are not sufficiently represented.

3 UV rheometry

3.1 Experimental setup

To investigate the change in the viscoelastic properties of the photopolymer resin during the curing process below the gelation point, a conventional rheometer (AR G2 provided by TA Instruments) was upgraded with the UV-curing

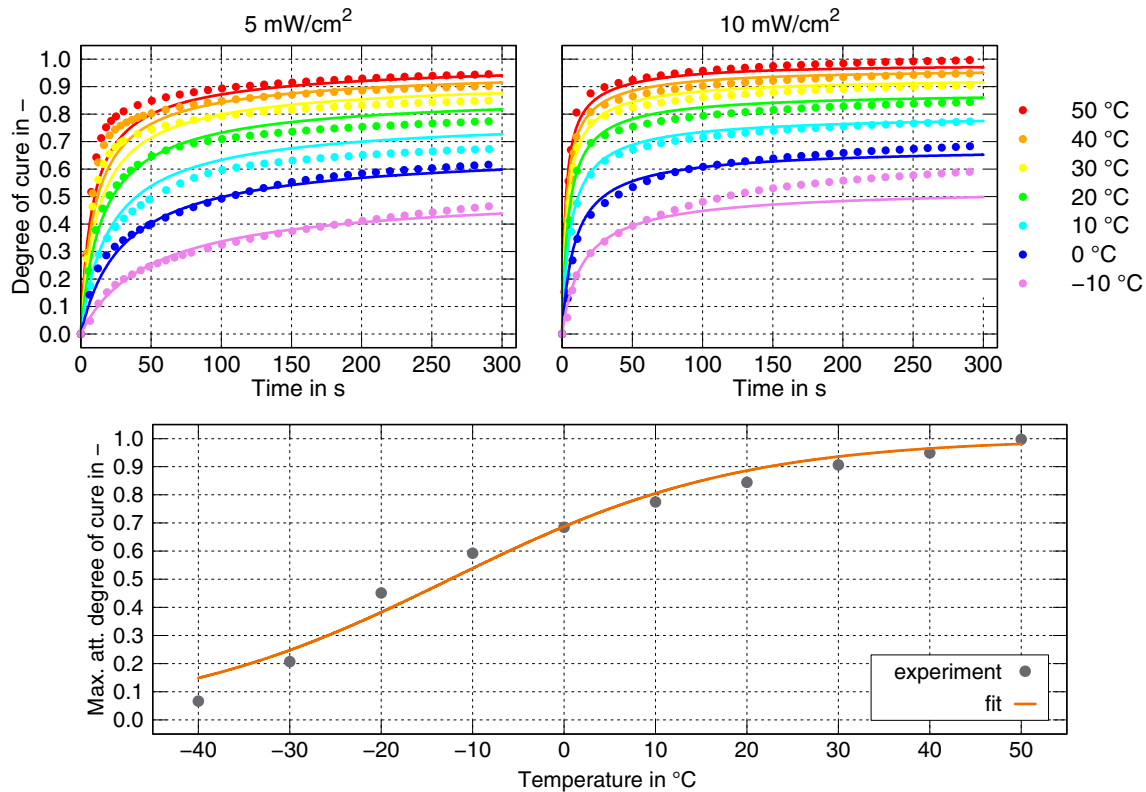


Fig. 2 Top: experimental results of the photo-DSC measurements for various isothermal conditions (dots) and comparison with the model equation of the evolution of the degree of cure q (solid lines). Bot-

tom: fit of the function $q_{\max}(\theta)$ for the threshold value depending on the curing temperature

Table 1 Parameters of the model equation for the degree of cure q

Parameter	Value	Unit	Description
A_1	0.6624	1/s	Pre-exponential factor of the first Arrhenius coefficient
A_2	0.6523	1/s	Pre-exponential factor of the second Arrhenius coefficient
E_1	12320	J/mol	Activation energy of the first Arrhenius coefficient
E_2	7994	J/mol	Activation energy of the second Arrhenius coefficient
m	30.85	–	Exponent of the first reaction
n	2.271	–	Exponent of the second reaction
b	1.794	–	Scaling factor of the influence of the light intensity
θ_0	-12.47	°C	Scaling coefficient of the fit function $q_{\max}(\theta)$
a_0	0.063	1/°C	Scaling coefficient of the fit function $q_{\max}(\theta)$
h_{tot}	-319.73	J/g	Total specific heat of reaction

accessory. Hence, the rheometric measurements were conducted during the curing process under UV irradiation. This equipment contains the same light source as used for the photo-DSC measurements and a quartz plate with a diameter of 20 mm. The light intensity is calibrated using a portable radiometer.

A schematic representation of the experimental setup and the curing progress in the photopolymer layer with layer thickness h_0 is depicted in Fig. 3, while the latter one is described in detail in the following. At the beginning ($t = t_0$), the photopolymer layer is a static fluid and fully liquid (a). After 120 s of conditioning the photopolymer layer with the sinusoidal shear excitation $\gamma(t) = \hat{\gamma} \sin(\omega t)$ with constant angular frequency ω and amplitude $\hat{\gamma}$, the shutter of the UV light source is opened and the curing reaction starts while continuing the shear excitation. Then, after exposure with time t_1 , the photopolymer layer starts to solidify at the bottom (b). From this point on, the crosslinking proceeds in the vertical direction (c) and, eventually, results in a

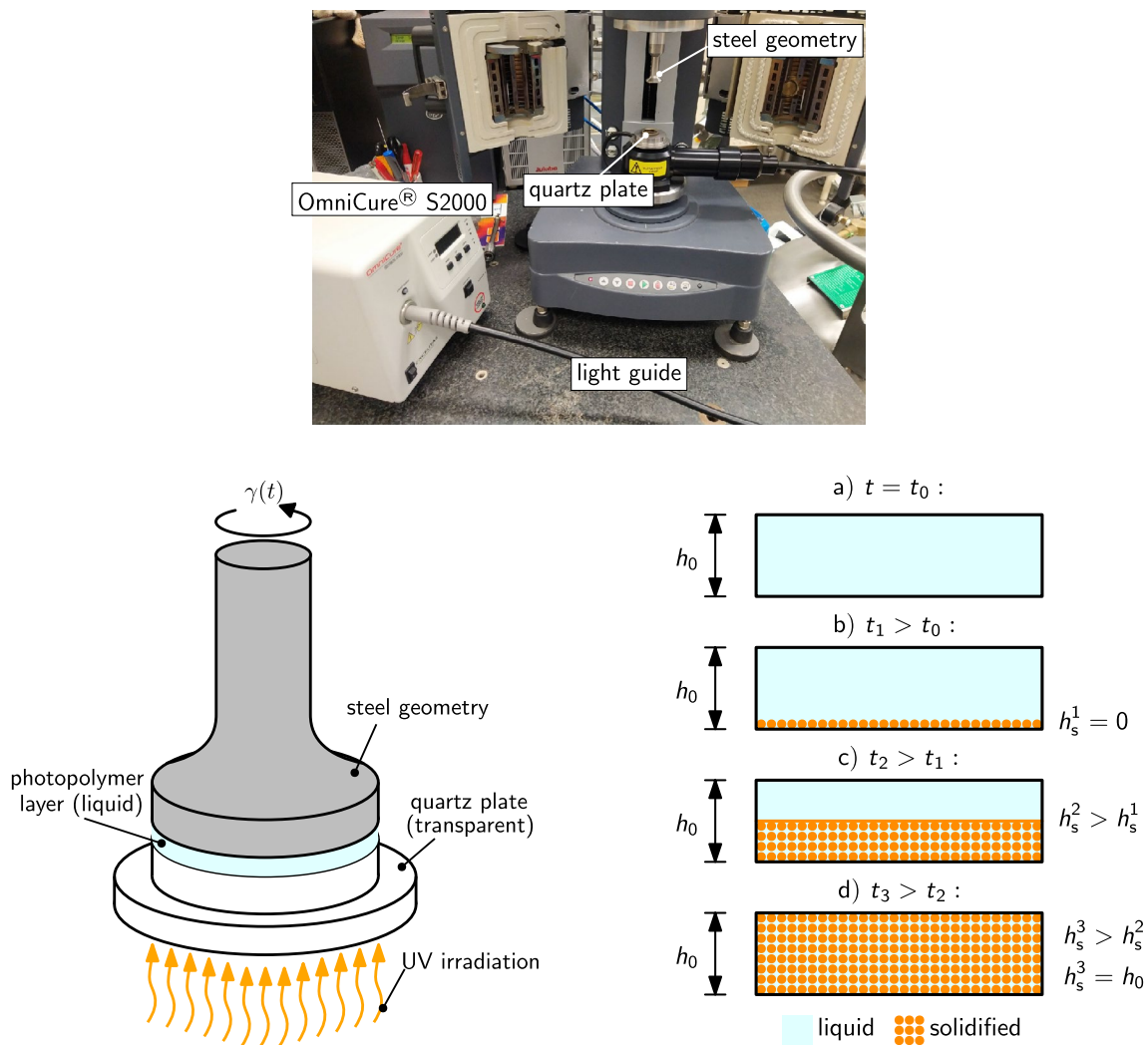


Fig. 3 Top: experimental setup of the UV rheometry test. Bottom left: Schematic representation of the experimental setup for the rheometric measurements during the curing process. Bottom right: Curing

fully solidified photopolymer layer (d). At this point ($h_s^3 = h_0$), the contact between the upper steel geometry and the photopolymer layer is established, so that the rheometer can measure the evolution of the storage and the loss modulus. Additionally, due to the internal measurement system of the rheometer, the chemical shrinkage in the vertical direction with progressing degree of cure is detected when the curing front reaches the upper steel geometry.

3.2 Working curve

Based on the Beer–Lambert law, Jacobs [26] developed the working curve equation by which two important parameters of photopolymer crosslinking can be identified

progress initiated by incident UV irradiation on the bottom side of the photopolymer layer

$$h_s = D_p \ln \left(\frac{E_0}{E_c} \right)$$

h_s : solidified layer thickness

D_p : penetration depth

E_c : critical exposure for solidification

E_0 : exposure for solidification of a layer with thickness h_s . (5)

This equation describes how much exposure E_0 is needed to solidify a photopolymer layer with layer thickness h_s . The two important parameters are the penetration depth D_p , which is the slope of the working curve equation in a semi-logarithmic representation and the critical exposure for solidification E_c at which the working curve intersects the abscissa.

Moreover, it is noted that the critical exposure E_c needed to start the solidification of the photopolymer corresponds to the gelation point of the photopolymer. The gelation point is described as the state at which a crosslinking polymer passes from a fluid into a solid [27]. This yields to a method of determination of the degree of cure at the gelation point of the photopolymer at which the equilibrium stiffness is established. For this purpose, the reaction kinetics model is linked with the information from the working curve.

To generate the working curve, several samples with various layer thicknesses and light intensities were cured using the UV rheometry setup. Depending on the layer thickness and light intensity, the time until the start of the detection of increasing storage and loss modulus is measured and multiplied with the light intensity, so that one obtains the light exposure needed to solidify the photopolymer layer. The results of these tests are depicted in Fig. 4 and fitted with the working curve equation in Eq. 5. The corresponding values of the parameters are listed in Table 2.

If one combines the model equation of the degree of cure with the parameter E_c of the corresponding working curve, one can determine the time needed to achieve the critical exposure, so that the photopolymer gels. Using this information, the corresponding degree of cure at the gelation point q_{gel} follows. Applying this procedure results in a value of $q_{gel} = 0.37$.

3.3 Time-cure superposition below the gelation point

To complete the evaluation of the UV rheometer test, the evolution of the shear storage modulus due to the curing as a function of the different test frequencies must also be considered. To obtain a preferably large database, measurements were carried out at four different angular frequencies

Table 2 Parameters of the working curve equation of the Loctite® 3D 3830 resin generated through the OmniCure® S2000 curing system

Parameter	Value	Unit
E_c	35.2	mJ/cm ²
D_p	308.97	μm

($\omega = 0.628$ rad/s, 6.28 rad/s, 62.8 rad/s, and 628 rad/s), one light intensity ($\mathcal{I} = 4.68$ mW/cm²) and ambient temperature ($\theta = 20$ °C). The corresponding curves are shown in the form of the shear storage modulus in Fig. 5 and exhibit the following two characteristics:

- After starting the irradiation, the shear storage modulus increases in all measurements with progressing degree of cure.
- Higher angular frequencies lead to higher shear storage modulus. With increasing degree of cure or time, the difference between the curves belonging to the different angular frequencies in the semi-logarithmic representation decreases.

After measuring the shear storage modulus, the experimental data in the time domain are linked to the model equations for the degree of cure (Eqs. 2–4) for the given test conditions. This results in subcurves depending on the degree of cure of the shear storage modulus in the frequency domain, see Fig. 6. These sub curves are then shifted manually to a continuous master curve at the reference degree of cure $q = 0.62$. The corresponding exponents to base 10 of the shift factors are also displayed in Fig. 6 leading to the master curve in Fig. 7. In the later following Sect. 4.4, the model equation for these shift factors is introduced and fitted to the test data at hand.

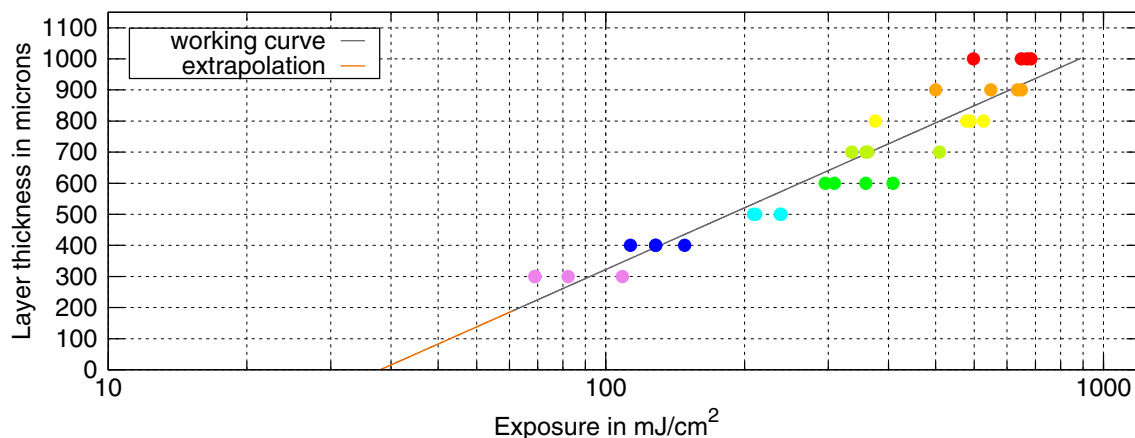


Fig. 4 Working curve of the Loctite 3D 3830 photopolymer resin. The data points were generated by measuring the time needed to start the crosslinking process in the UV rheometry test using the OmniCure® S2000 curing system

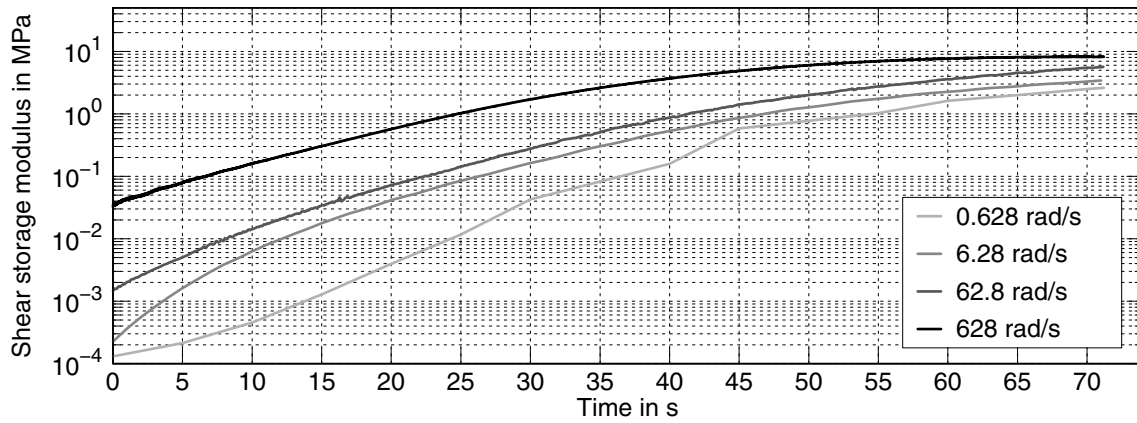


Fig. 5 Evolution of the shear storage modulus in the UV rheometer tests under various test frequencies

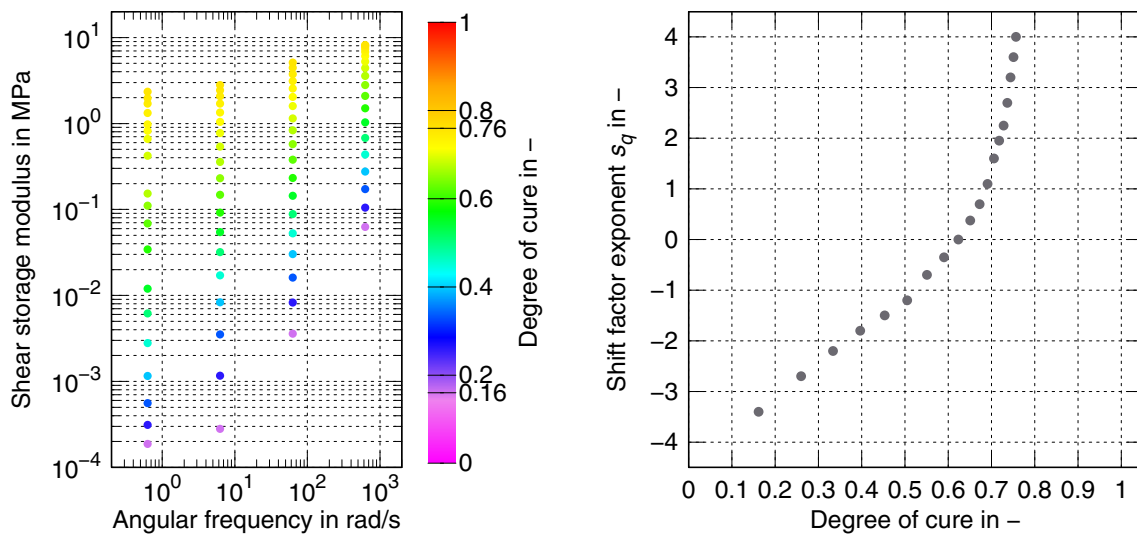


Fig. 6 Left: transformation of the curves of the shear storage modulus in Fig. 5 into the frequency domain using the model equation of the degree of cure at various constant degree of cure. The lowest and highest curves correspond to the degrees of cure $q = 0.16$

and $q = 0.76$, respectively. Right: shift factor exponents to base 10 depending on the degree of cure for the generation of the master curve based on the UV rheometer tests

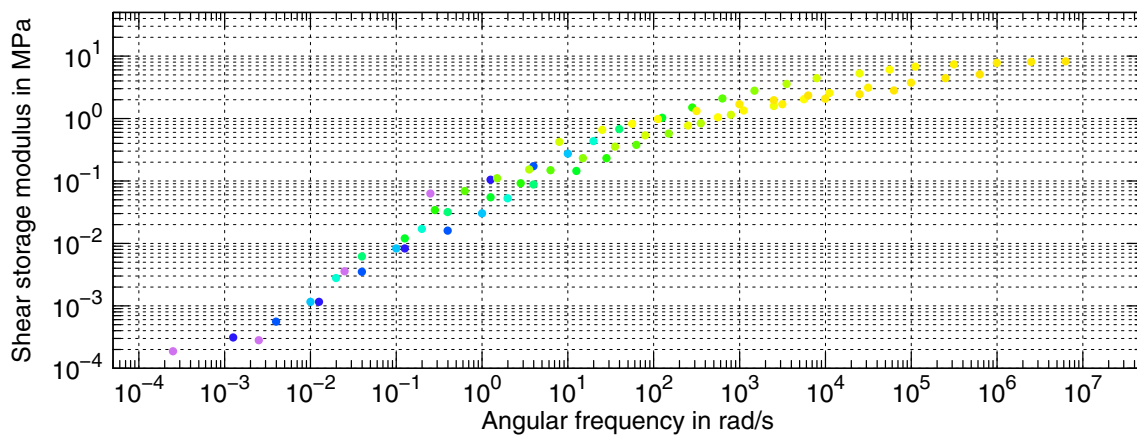


Fig. 7 Resulting master curve after shifting the subcurves of Fig. 6 at constant degree of cure $q = 0.62$

4 Dynamic-mechanical analysis

4.1 Experimental setup

Dynamic-mechanical analysis (DMA) is an established procedure to characterize the viscoelastic behavior of (photo-)polymers in the frequency domain. For example, Reichl and Inman [28] investigated the viscoelastic behavior of photopolymer samples depending on the print direction and fabricated by the Objet Connex 500 printer provided by Stratasys®.

The rheometer AR G2 provided by TA Instruments was used to carry out the tests in this paper. Several cylindrical rods were printed with different exposure times (1.5 s, 2 s, 3 s, and 4 s) per layer (layer thickness $\delta = 50 \mu\text{m}$) by the Loctite® DLP 3D printer to generate various conditions with regard to the degree of cure.

Table 3 Resulting degree of cure of the samples for the DMA tests depending on the exposure time for each layer

Exposure time per layer in s	1.5	2	3	4
Degree of cure q in -	0.82	0.87	0.90	0.96

Moreover, a small sample ($\sim 5 \text{ mg}$) was cut out of the middle of each sample for a subsequent photo-DSC scan to determine the residual enthalpy of reaction and consequently the degree of cure of each sample that are listed in Table 3.

Afterwards, a harmonic shear excitation is applied to the top of the cylindrical rod specimen whereas the bottom is fixed—see Fig. 8

$$\gamma(t) = \hat{\gamma} \sin(\omega t). \quad (6)$$

Ensuring the assumption of infinitesimal strains for linear viscoelasticity, the amplitude is chosen as $\hat{\gamma} = 0.05\%$. The rheometer measures the torque $M(t)$ during oscillation and calculates the shear stress $\tau(t)$ at the edge of the specimen that is inhomogeneously distributed over the radius based on the given geometry. Due to the viscoelastic behavior of the cured photopolymer resin, the shear stress is phase-shifted to the applied shear excitation—see Fig. 8

$$\tau(t) = \hat{\tau} \sin(\omega t + \delta). \quad (7)$$

Herein, δ denotes the phase-shift angle that is used for the calculation of the loss factor $\tan \delta$. Generally, due to the temperature and frequency dependence of the photopolymer, the phase-shift angle depends on the mentioned variables. To calculate the complex shear modulus that is used for the

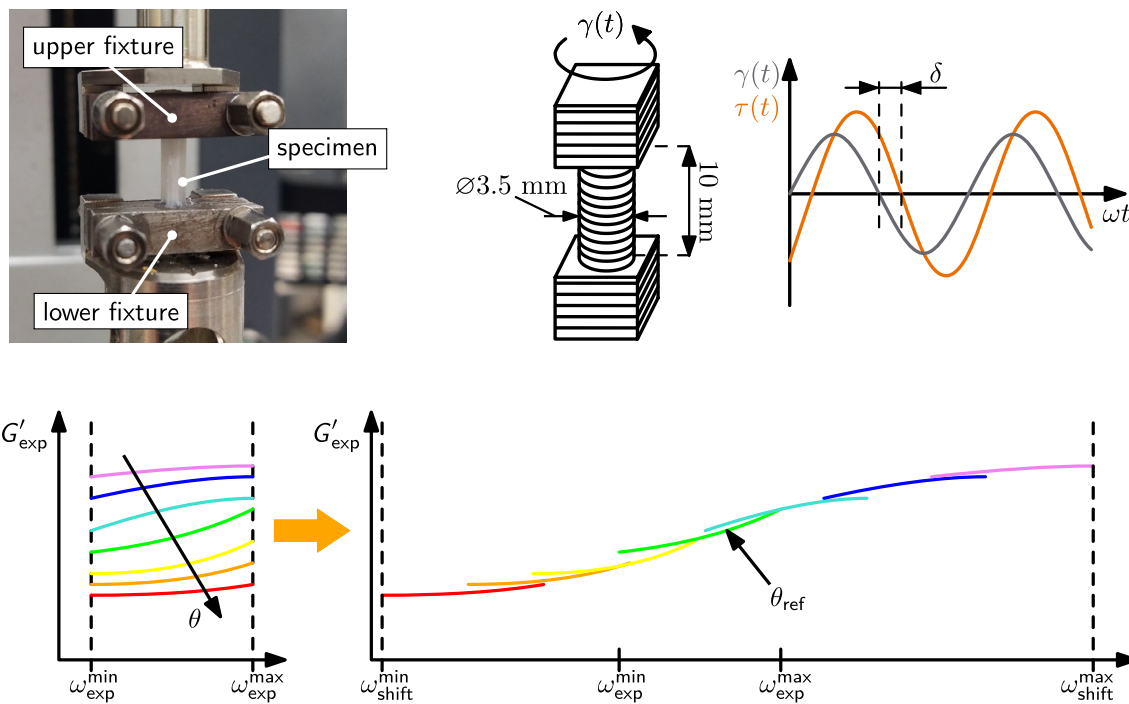


Fig. 8 Top: experimental setup of the DMA test in torsional mode; the bottom of the cylindrical rod is fixed, whereas the shear excitation is applied to the top by the upper fixture (the layer orientation is

indicated by the hatching of the sample). Bottom: schematic representation of the time-temperature superposition of the shear storage modulus

later following parameter identification, the stress and the strain are transferred into complex variables:

$$\gamma^*(t) = \hat{\gamma} \exp(i\omega t) \tag{8}$$

$$\tau^*(t) = \hat{\tau} \exp(i(\omega t + \delta)). \tag{9}$$

The experimental complex shear modulus $G^*(\omega)$ for a given angular frequency ω is then computed as

$$G^*(\omega) = \frac{\tau^*(t)}{\gamma^*(t)} = \underbrace{\hat{\tau}}_{=:G'} \cos(\delta) + i \cdot \underbrace{\hat{\tau}}_{=:G''} \sin(\delta) \tag{10}$$

with the shear storage modulus $G'(\omega)$ as the real part (in phase) and the shear loss modulus $G''(\omega)$ as the imaginary part (out of phase) [29]. In this representation, both variables depend only on the amplitudes $\hat{\tau}$ and $\hat{\gamma}$ and the phase-shift angle δ and therefore on the frequency of excitation.

4.2 Time-temperature superposition

Figure 8 (bottom) shows the general concept of time-temperature superposition. For thermoreologically simple materials, the effect of a temperature change can also be caused by a change in loading frequency or loading speed: higher temperatures lead to the same material behavior as lower loading frequencies and vice versa. Using this analogy, the time-temperature superposition principle is performed: in a diagram with a logarithmic frequency axis, one chooses the isothermal curve of the shear storage modulus at one

reference temperature θ_{ref} and shifts the other isothermal curves of higher (lower) temperatures to lower (higher) frequencies, so that the experimental frequency range is extended by several decades. Ideally, the shifted isothermal curves produce a continuous curve that is called the master curve and which is used for the identification of the parameters for the description of the viscoelastic behavior at the reference temperature. Afterwards, the parameters can be shifted to a different temperature using a suitable shift function.

At several temperatures, starting at $-100\text{ }^\circ\text{C}$ and going up to $300\text{ }^\circ\text{C}$, the harmonic shear excitation in Eq. 6 is applied on the sample with various angular frequencies ($\omega = 6.28\text{ rad/s} \dots 188.5\pi\text{ rad/s}$). The corresponding courses of the shear storage modulus G' calculated from the isothermal frequency sweeps are shown in Fig. 9 for the four different samples. In addition to the strong temperature dependence of the shear storage modulus in each plot, three other important phenomena can be identified

- The equilibrium stiffness, which corresponds to the frequency independent material response at high temperatures, decreases with decreasing degree of cure.
- The instantaneous material response is independent of the degree of cure. This behavior is indicated by the frequency independent shear storage modulus at the lowest temperature ($G' \approx 2000\text{ MPa}$).
- The lower the degree of cure the lower and more frequency dependent is the shear storage modulus at constant temperature compared to higher degrees of cure.

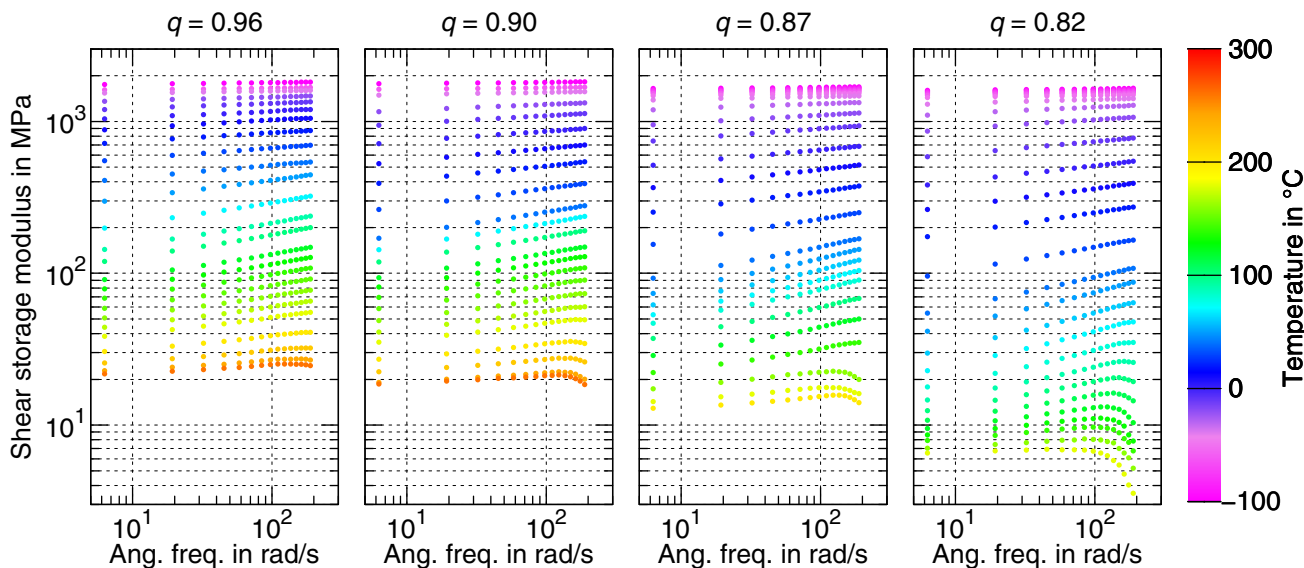


Fig. 9 Isothermal curves of the shear storage modulus G' obtained from the DMA tests depending on the degree of cure. For a better representation, the selection of isothermal curves is based on the visibility of the increase of the shear storage modulus

All these phenomena combined indicate that the time-temperature superposition principle may be applied. Unfortunately, some of the specimens broke during the test due to the elevated temperature, which resulted in the descending courses at higher temperatures and frequencies. Nevertheless, the experimental database is sufficient to generate a master curve based on the isothermal curves for each degree of cure.

The corresponding exponents to base 10 of the shift factors for the generation of the master curves for each degree of cure at the reference temperature $\theta_{\text{ref}} = 20^\circ\text{C}$ using the time-temperature superposition principle are displayed in Fig. 10 and fitted through the Williams–Landel–Ferry (WLF) equation [30]

$$s_\theta(\theta) = \frac{-C_1(\theta - \theta_{\text{ref}})}{C_2 + (\theta - \theta_{\text{ref}})} \quad (11)$$

The WLF equation was adapted by simultaneously considering all four different data sets of the shift factors and with the help of the Levenberg–Marquardt algorithm implemented in

the software gnuplot. The parameters resulted in $C_1 = 32.73$ and $C_2 = 448.62^\circ\text{C}$.

It should be noted that, taking into account measurement inaccuracies that occur, the experimental shift factors are almost independent of the degree of cure. This is an important fact leading to the conclusion that the time-temperature superposition principle can be modeled independently of the time-cure superposition principle in Sect. 3.

4.3 Identification of relaxation times and stiffnesses at the reference point

In general, the mechanical response of polymers depends on time, temperature, and degree of cure, see [31]. To model this behavior, the following relation is introduced for the relaxation times τ_i :

$$\tau_i(\theta, q) = \tau_i^{\text{ref}} \cdot 10^{s_\theta(\theta) + s_q(q)} \quad (12)$$

The relaxation times τ_i^{ref} are chosen at an appropriate reference point. $s_\theta(\theta)$ and $s_q(q)$ are suitable shift functions whereby the former one is described by Eq. 11.

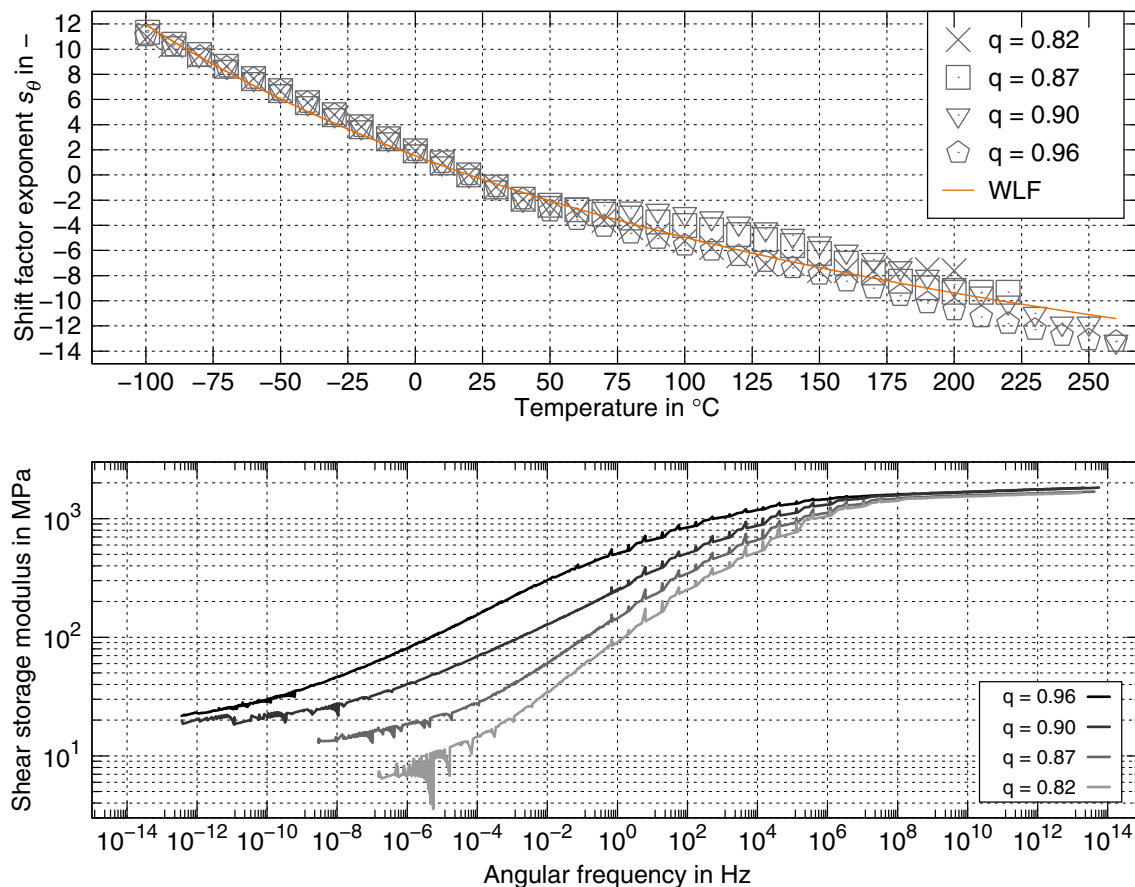
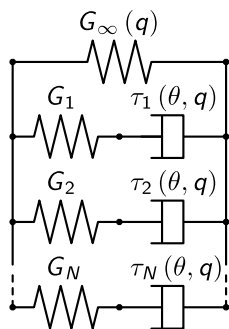


Fig. 10 Top: shift factor exponents to base 10 of the time-temperature superposition for the generation of the master curves depending on the degree of cure q . Bottom: resulting master curves after shifting the isothermal curves in Fig. 9 depending on the degree of cure

Fig. 11 Rheological network of the deviatoric part of the generalized Maxwell model



For the representation of the measured shear storage modulus, the generalized Maxwell model as depicted as the rheological network in Fig. 11 is assumed. Applying standard calculations, one obtains the following relation for the shear storage modulus G' [32]:

$$G'(\omega, G_i, \tau_i) = G_\infty(q) + \sum_{i=1}^N G_i \frac{(\omega\tau_i(\theta, q))^2}{1 + (\omega\tau_i(\theta, q))^2} \tag{13}$$

Herein, the equilibrium stiffness $G_\infty(q)$ is formulated as a function of the degree of cure. Using this approach, the stiffnesses G_i are kept constant, so that all dependencies are captured by the temperature- and degree of cure-dependent relaxation times τ_i . Moreover, for the pre-gel state of the resin (i.e., $G_\infty(q < q_{gel}) = 0$), the model yields to a parallel arrangement of the single Maxwell chains that describes fluid-like behavior.

The identification procedure of the relaxation times and stiffness is conducted stepwise, once more using LS-OPT[®]. At first, the stiffnesses G_i , relaxation times τ_i , and equilibrium modulus G_∞ at the reference point

($q_{ref} = 0.96 \mid \theta_{ref} = 20 \text{ }^\circ\text{C}$) are identified. To do this, the master curve of the DMA test at the reference conditions is considered as the objective.

Before starting the identification procedure, the experimental frequency range of the master curve is divided into subdomains, so that each relaxation time covers one decade. The upper and lower bounds of the relaxation times are each set 1 decade away from the start value. The stiffnesses G_i are initially set to 100 MPa .

For a better representation of the experimental data in a log–log scale as depicted in Fig. 12, the Mean Squared Logarithmic Error (MSLE) is used as a criterion for the evaluation of the model parameters

$$MSLE = \frac{1}{R} \sum_{j=1}^R \left(\log_{10} G'_{sim,i}(\mathbf{x}) - \log_{10} G'_{exp,i} \right)^2 \tag{14}$$

R is the number of regression points

$G'_{sim,i}$ is the simulated shear storage modulus at regression point i
 $G'_{exp,i}$ is the experimental shear storage modulus at regression point i

\mathbf{x} is the vector of design variables.
 tors of design variables \mathbf{x} include the relaxation times t_i^{ref} , equilibrium stiffness $G_\infty(q_{ref})$, and stiffnesses G_i . Compared to the standard mean squared error, the MSLE has the advantage that a consistent weighting of the deviation is performed between experimental and simulated values regardless of the value of the abscissa. This is especially important for data sets like frequency-dependent storage moduli that increase over many decades.

The result of the identification of the viscoelastic spectrum at the reference point is depicted in Fig. 12 as a comparison between the simulated and the measured storage modulus (see also Table 4 for the identified parameters).

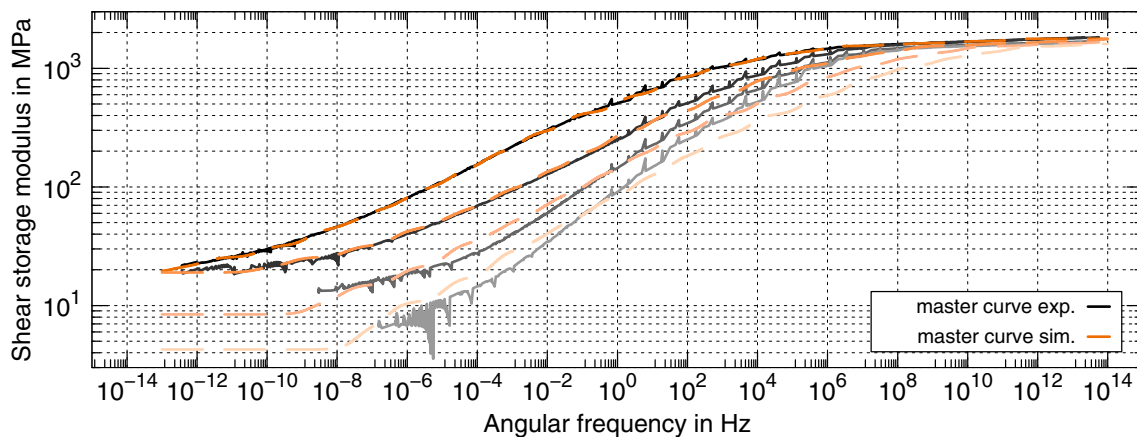


Fig. 12 Simulation of the generalized Maxwell model using several master curves depending on the degree of cure

Table 4 Identified stiffnesses G_i and relaxation times τ_i^{ref} at the reference point $\theta_{\text{ref}} = 20^\circ\text{C}$, $q_{\text{ref}} = 0.96$

i	Stiffness G_i in MPa	Relaxation time τ_i^{ref} in s
1	2.36	$5.083 \cdot 10^{12}$
2	4.158	$6.122 \cdot 10^{11}$
3	6.404	$1.521 \cdot 10^{10}$
4	12.08	$6.204 \cdot 10^8$
5	7.677	$5.885 \cdot 10^7$
6	13.56	$1.362 \cdot 10^7$
7	16.66	$1.628 \cdot 10^6$
8	17.67	$5.185 \cdot 10^5$
9	41.58	$5.626 \cdot 10^4$
10	59.19	5408
11	91.71	478.8
12	132.1	28.46
13	174.2	0.9977
14	236.7	0.05175
15	69.89	0.005159
16	157.1	0.002508
17	189.8	0.000152
18	121.9	$1.583 \cdot 10^{-5}$
19	172.3	$1.328 \cdot 10^{-6}$
20	22.13	$3.535 \cdot 10^{-8}$
21	41.24	$1.191 \cdot 10^{-8}$
22	22.85	$3.062 \cdot 10^{-9}$
23	59.17	$2.228 \cdot 10^{-10}$
24	86.19	$6.1 \cdot 10^{-12}$

4.4 Time-cure superposition beyond the gelation point

In the next step of the identification procedure, the identified relaxation times are shifted by a factor for each master curve in Fig. 10. Additionally, the equilibrium stiffness G_∞ is considered as degree of cure-dependent, so that two parameters are identified for each master curve.

The results of the second step of the parameter identification are also displayed in Fig. 12 as a comparison between the experimental master curves and the simulations. Compared to the reference at $q = 0.96$, the MSLE increases with decreasing degree of cure, see Table 5. Additionally, the identified equilibrium stiffnesses are listed in Table 6 and also show a strong dependence on the degree of cure.

Finally, the shifting results below the gelation point from the UV rheometry measurements have to be combined with the time-cure shift factors of the DMA measurements. For this purpose, the shift factors in Fig. 6 are related to the reference degree of cure ($q = 0.96$) by manually shifting the factors vertically, so that they form

Table 5 MSLE between experimental mastercurves and simulation results depending on the degree of cure q

Degree of cure q in -	MSLE in -
0.82	$1.9 \cdot 10^{-3}$
0.87	$4.8 \cdot 10^{-4}$
0.90	$1.2 \cdot 10^{-4}$
0.96	$8.4 \cdot 10^{-6}$

Table 6 Degree of cure-dependent equilibrium stiffness $G_\infty(q)$

Degree of cure q in -	0.96	0.90	0.87	0.82
G_∞ in MPa	19.01	19.0	8.41	4.26

Table 7 Parameters of the time-cure shift function $s_q(q)$ proposed by Eom et al. [13]

Parameter	s_{q1}	s_{q2}	s_{q3}	$s_{q_{\text{gel}}}$
Value in -	6.81	23.03	1.78	-14.96

a continuous curve with the shift factors from the DMA measurements.

For the mathematical representation of the time-cure shift factors, the approach proposed by Eom et al. [13] is applied

$$s_q(q) = \begin{cases} s_{q1}(q - q_{\text{gel}}) + s_{q_{\text{gel}}} & , q < q_{\text{gel}} \\ s_{q_{\text{gel}}} \cdot s_{q2}^{(q - q_{\text{gel}})} \left(\frac{1 - q}{1 - q_{\text{gel}}} \right)^{s_{q3}} & , q \geq q_{\text{gel}} \end{cases} \quad (15)$$

The parameters used herein are dimensionless and $s_{q_{\text{gel}}}$ denotes the shift factor at the gelation point. Using the software gnuplot again, the parameters are identified for the pre-gelation and post-gelation domain, respectively, and are listed in Table 7. Figure 13 shows the identification result, which indicates a good representation of the time-cure shift factors using Eq. 15.

5 Conclusion and outlook

In the present paper, the following experimental investigations are performed to characterize the viscoelastic properties of the commercial photopolymer resin Loctite[®] 3D 3830 used in digital light processing:

- Photo-DSC for measuring the curing reaction and modeling the evolution of the degree of cure depending on temperature and light intensity
- UV rheometry for the measurement of the evolution of the shear storage modulus in the gel–sol transition and

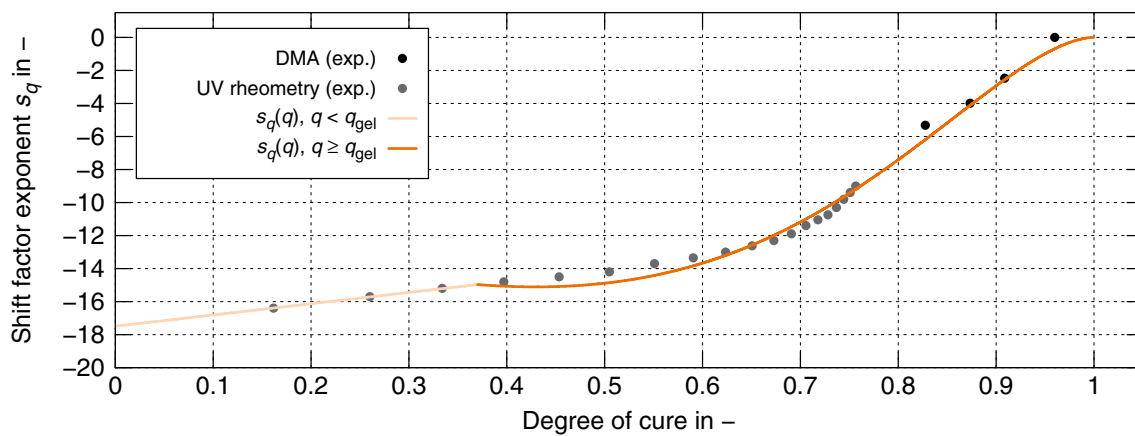


Fig. 13 Graphical representation and fitting of the time-cure shift factors under the usage of Eq. 15

generation of the working curve for the determination of the gelation point

- Dynamic-mechanical analysis of printed specimens for the experimental determination of the shear storage modulus beyond the gelation point.

Based on the experimental results, suitable model equations are developed taking into account established approaches from various literature.

Time-temperature and time-cure superposition principles are applied to cover the temperature- and degree of cure-dependent viscoelastic properties of the considered photopolymer. It is shown that the temperature, as well as the degree of cure, have a significant influence on the viscoelastic properties and that both phenomena can be modeled independently. This also leads to the fact that the application of a purely elastic material model is insufficient in finite-element simulations under various conditions.

The parameters of the model equations were identified using the commercial optimization program LS-OPT® leading to a good representation of the experimental data. The findings of this paper help users in additive manufacturing of photopolymers using DLP to predict the mechanical properties of the material depending on several parameters before starting the print job. If the change of the mechanical properties is considered during the curing process, it is also possible to estimate the peeling forces acting on the printed layers when they are detached from the resin tray. Otherwise, the print job can fail due to excessive peeling forces.

Future considerations will lead to the development of a three-dimensional material model that is capable of predicting the material response under various conditions and printing parameters. To do this, the rheological network in Fig. 11 is extended by an additional part for the bulk behavior. The three-dimensional material model in conjunction with the experimental techniques shown in this paper can

then be used for the optimization of the printing process using simulations.

Acknowledgements The financial support of the project “Constitutive modeling of UV-curing printed polymer composites” by the German Research Foundation (DFG) and Agence nationale de la recherche (ANR) under the grant numbers LI 696/20-1 and ANR-18-CE92-0002-01 is gratefully acknowledged.

Funding Open Access funding enabled and organized by Projekt DEAL.

Declarations

Conflict of interest On behalf of all authors, the corresponding author states that there is no conflict of interest

Open Access This article is licensed under a Creative Commons Attribution 4.0 International License, which permits use, sharing, adaptation, distribution and reproduction in any medium or format, as long as you give appropriate credit to the original author(s) and the source, provide a link to the Creative Commons licence, and indicate if changes were made. The images or other third party material in this article are included in the article’s Creative Commons licence, unless indicated otherwise in a credit line to the material. If material is not included in the article’s Creative Commons licence and your intended use is not permitted by statutory regulation or exceeds the permitted use, you will need to obtain permission directly from the copyright holder. To view a copy of this licence, visit <http://creativecommons.org/licenses/by/4.0/>.

References

1. Eng H, Maleksaeedi S, Yu S (2017) Development of cnts-filled photopolymer for projection stereolithography. *Rapid Prototyp J* 23(1):129–136
2. Bennett J (2017) Measuring UV curing parameters of commercial photopolymers used in additive manufacturing. *Addit Manuf* 18:203–212
3. Wu J, Zhao Z, Hamel CM, Mu X, Kuang X, Guo Z, Qi HJ (2018) Evolution of material properties during free radical

- photopolymerization. *J Mech Phys Solids* 112:25–49. <https://doi.org/10.1016/j.jmps.2017.11.018>
4. Yang Y, Li L, Zhao J (2019) Mechanical property modeling of photosensitive liquid resin in stereolithography additive manufacturing: bridging degree of cure with tensile strength and hardness. *Mater Des* 162:418–428
 5. Weeger O, Boddeti N, Yeung SK, Kaijima S, Dunn M (2019) Digital design and nonlinear simulation for additive manufacturing of soft lattice structures. *Addit Manuf* 25:39–49
 6. Hossain M, Liao Z (2020) An additively manufactured silicone polymer: Thermo-viscoelastic experimental study and computational modelling. *Addit Manuf* 35:101395. <https://doi.org/10.1016/j.addma.2020.101395>
 7. Hossain M, Navaratne R, Perić D (2020) 3d printed elastomeric polyurethane: viscoelastic experimental characterizations and constitutive modelling with nonlinear viscosity functions. *Int J Non-Linear Mech* 126:103546. <https://doi.org/10.1016/j.ijnonlinmec.2020.103546>
 8. Cheah C, Fuh J, Nee A, Lu L, Choo Y, Miyazawa T (1997) Characteristics of photopolymeric material used in rapid prototypes Part II. Mechanical properties at post-cured state. *J Mater Process Technol* 67(1):46–49
 9. Monzón M, Ortega Z, Hernández A, Paz R, Ortega F (2017) Anisotropy of photopolymer parts made by digital light processing. *Materials* 10(1):64
 10. Hong SY, Kim YC, Wang M, Kim HI, Byun DY, Nam JD, Chou TW, Ajayan PM, Ci L, Suhr J (2018) Experimental investigation of mechanical properties of uv-curable 3d printing materials. *Polymer* 145:88–94
 11. da Silva Bartolo PJ (2007) Photo-curing modelling: direct irradiation. *Int J Adv Manuf Technol* 32:480–491
 12. Westbeek S, Remmers J, van Dommelen J, Geers M (2020) Multi-scale process simulation for additive manufacturing through particle filled vat photopolymerization. *Comput Mater Sci* 180:109647
 13. Eom Y, Boogh L, Michaud V, Sunderland P, Manson JA (2000) Time-cure-temperature superposition for the prediction of instantaneous viscoelastic properties during cure. *Polym Eng Sci* 40(6):1281–1292
 14. Karalekas D, Aggelopoulos A (2003) Study of shrinkage strains in a stereolithography cured acrylic photopolymer resin. *J Mater Process Technol* 136(1):146–150. [https://doi.org/10.1016/S0924-0136\(03\)00028-1](https://doi.org/10.1016/S0924-0136(03)00028-1)
 15. Wu D, Zhao Z, Zhang Q, Qi HJ, Fang D (2019) Mechanics of shape distortion of DLP 3D printed structures during UV post-curing. *Soft Matter* 15:6151–6159. <https://doi.org/10.1039/c9sm00725c>
 16. Obst P, Riedelbauch J, Oehlmann P, Rietzel D, Launhardt M, Schmölzer S, Osswald TA, Witt G (2020) Investigation of the influence of exposure time on the dual-curing reaction of rpu 70 during the dls process and the resulting mechanical part properties. *Addit Manuf* 32:101002. <https://doi.org/10.1016/j.addma.2019.101002>
 17. Dizon JRC, Espera AH, Chen Q, Advincula RC (2018) Mechanical characterization of 3d-printed polymers. *Addit Manuf* 20:44–67. <https://doi.org/10.1016/j.addma.2017.12.002>
 18. Klikovits N, Sinaweil L, Knaack P, Koch T, Stampfl J, Gorsche C, Liska R (2020) Uv-induced cationic ring-opening polymerization of 2-oxazolines for hot lithography. *ACS Macro Lett* 9(4):546–551
 19. Steyrer B, Busetti B, Harakály G, Liska R, Stampfl J (2018) Hot lithography vs. room temperature dlp 3d-printing of a dimethacrylate. *Addit Manuf* 21:209–214
 20. Henkel Corporation, Rocky Hill: LOCTITE 3D 3830 CL Safety Data Sheet (2017)
 21. Rehbein T, Lion A, Johlitz M, Constantinescu A (2020) Experimental investigation and modelling of the curing behaviour of photopolymers. *Polym Test* 83:106356. <https://doi.org/10.1016/j.polymertesting.2020.106356>
 22. Kamal MR, Sourour S (1973) Kinetics and thermal characterization of thermoset cure. *Polym Eng Sci* 13(1):59–64. <https://doi.org/10.1002/pen.760130110>
 23. Hossain M, Possart G, Steinmann P (2009) A small-strain model to simulate the curing of thermosets. *Comput Mech* 43:769–779
 24. Hossain M, Saxena P, Steinmann P (2015) Modelling the mechanical aspects of the curing process of magneto-sensitive elastomeric materials. *Int J Solids Struct* 58:257–269. <https://doi.org/10.1016/j.ijsolstr.2015.01.010>
 25. Hossain M, Steinmann P (2015) Chapter three—continuum physics of materials with time-dependent properties: reviewing the case of polymer curing. Elsevier, Amsterdam, pp 141–259
 26. Jacobs PF (1992) Rapid Prototyping and manufacturing: fundamentals of stereolithography. *Soc Manuf Eng*
 27. Lange J, Månson JAE, Hult A (1996) Build-up of structure and viscoelastic properties in epoxy and acrylate resins cured below their ultimate glass transition temperature. *Polymer* 37(26):5859–5868
 28. Reichl K, Inman D (2018) Dynamic mechanical and thermal analyses of objet connex 3d printed materials. *Exp Tech* 142:19–25. <https://doi.org/10.1007/s40799-017-0223-0>
 29. Findley WN, Lai JS, Onaran K (1976) Creep and relaxation of viscoelastic materials. Dover Publications, Mineola
 30. Williams ML, Landel RF, Ferry JD (1955) The temperature dependence of relaxation mechanisms in amorphous polymers and other glass-forming liquids. *J Am Chem Soc* 77:3701–3707. <https://doi.org/10.1021/ja01619a008>
 31. Ferry JD (1980) Viscoelastic properties of polymers. Wiley, Hoboken
 32. Tschoegl NW (1989) The phenomenological theory of linear viscoelastic behavior. Springer, Berlin

Publisher's Note Springer Nature remains neutral with regard to jurisdictional claims in published maps and institutional affiliations.